Theory of quasiparticle interference in mirror-symmetric two-dimensional systems and its application to surface states of topological crystalline insulators

Chen Fang,[1,2] Matthew J. Gilbert,[3,4] Su-Yang Xu,[2] B. Andrei Bernevig,[2] and M. Zahid Hasan[2]
[1]*Department of Physics, University of Illinois, Urbana, Illinois 61801-3080, USA*
[2]*Department of Physics, Princeton University, Princeton, New Jersey 08544, USA*
[3]*Department of Electrical and Computer Engineering, University of Illinois, Urbana, Illinois 61801, USA*
[4]*Micro and Nanotechnology Laboratory, University of Illinois, Urbana, Illinois 61801, USA*
(Received 25 December 2012; revised manuscript received 20 June 2013; published 30 September 2013)

We study symmetry-protected features in the quasiparticle interference (QPI) pattern of two-dimensional (2D) systems with mirror symmetries and time-reversal symmetry, around a single static point impurity. We show that, in the Fourier-transformed local density of states (FT-LDOS) $\rho(\mathbf{q},\omega)$, while the position of high-intensity peaks generically depends on the geometric features of the iso-energy contour at energy ω, the *absence* of certain peaks is guaranteed by the opposite mirror eigenvalues of the two Bloch states that are (i) on the mirror-symmetric lines in the Brillouin zone (BZ) and (ii) separated by scattering vector $\mathbf{q}$. We apply the general result to the QPI on the $\langle 001\rangle$ surface of the topological crystalline insulator $Pb_{1-x}Sn_xTe$ and predict all vanishing peaks in $\rho(\mathbf{q},\omega)$. The model-independent analysis is supported by numerical calculations using an effective four-band model derived from symmetry analysis.

DOI: 10.1103/PhysRevB.88.125141 PACS number(s): 73.20.At, 73.20.Hb

I. INTRODUCTION

Quantum interference is one of the simplest yet most fundamental quantum-mechanical phenomena. In condensed matter physics, the interference pattern of quasiparticles around a single impurity observed through scanning tunneling spectroscopy (STS) has been widely used for electronic structure characterization of unconventional states.[1,2] For instance, quasiparticle interference (QPI) has been applied to demonstrate the defining property of time-reversal symmetric (TRS) topological insulators:[3–8] the *absence* of backscattering in the surface states. In fact, a generic relationship between the absence of certain scattering channels and the underlying symmetry group exists in any system. In this paper, we elucidate such relations in two-dimensional (2D) systems with mirror symmetries by analyzing properties of the Fourier-transformed local density of states (FT-LDOS) around a single static impurity of an arbitrary kind (potential, magnetic, dipolar, etc.). We show that while generically the positions of high-intensity peaks of the FT-LDOS at a given energy are determined by the shape of the iso-energy contour,[9,10] peaks at $\rho(\mathbf{q},\omega)$ vanish if the two Bloch states separated by $\mathbf{q}$ on the contour have opposite mirror eigenvalues. Moreover, the inverse statement is also true: by identifying the absence of these peaks in a multiband system, we know that the two states mirror eigenvalues of each band on mirror-symmetric lines in the Brillouin zone (BZ), thus partly revealing the orbital nature of these bands. ("Orbital" includes orbital and spin degrees of freedom.)

The surface states of the recently discovered topological crystalline insulators (TCIs) make an example of a multi-orbital 2D metal. Among the intensive theoretical efforts on topological phases beyond those protected by time-reversal symmetry,[11–17] Hsieh *et al*. predicted,[15] via first-principles calculation, that SnTe is a nontrivial insulator whose topology is protected by mirror symmetries, dubbed a mirror-symmetric topological crystalline insulator (MSTCI), characterized by robust surface states on the $\langle 001\rangle$ plane which contains in the surface BZ four Dirac points (two along $\bar{X}$-$\bar{\Gamma}$-$\bar{X}$ and two along $\bar{Y}$-$\bar{\Gamma}$-$\bar{Y}$). This prediction has been experimentally confirmed[18–20] through the use of angle-resolved photoemission spectroscopy (ARPES) in $Pb_{1-x}Sn_xTe$. Furthermore,[18,20] as the binding energy increases away from the Dirac-point binding energy, the surface states undergo a Lifshitz transition at a critical energy E_c where the iso-energy contour changes from two separate ellipsoids to two concentric ellipsoids. Theoretical proposals of other types of TCI materials have also appeared.[21–23] The defining property of a MSTCI is that the surface Dirac point is protected by *mirror symmetry*, i.e., the two degenerate states at each Dirac point have different mirror eigenvalues. In this paper, we show that it can be promptly identified by examining the vanishing intensities in the FT-LDOS.

To numerically verify the theory, we use symmetry analysis to derive a minimal four-band model that semiquantitatively recovers the observed dispersion and the Lifshitz transition. We calculate the FT-LDOS around a point-charge impurity and see complete intensity suppression at wave vectors connecting two states with opposite mirror eigenvalues, even when the scattering is *not* forbidden by TRS.

The paper is organized as follows: In Sec. II, we develop a general analysis for the QPI in 2D systems with mirror symmetries and TRS, focusing on the general properties of the pattern and the symmetry-forbidden scattering channels in FT-LDOS. In Sec. III, we apply the general theory to the surface states of TCI SnTe, deducing all forbidden channels of FT-LDOS based on experimental facts only; then we develop an effective theory that captures the main features of the surface states and perform a numerical study which confirms our results. In Sec. IV, we discuss how the general theory can be applied to systems without spin-orbital coupling, where TRS-forbidden channels no longer exist and the limitations of our study.

(η_x,η_y,η_T)	Realization	Exact symmetries	Approximate relations	$\Sigma_{\alpha\beta}$
(1,1,1)	Point charge 	$\rho(q_x,q_y)=\rho(-q_x,q_y)$ $\rho(q_x,q_y)=\rho(q_x,-q_y)$		$\Sigma_{00},\Sigma_{10},\Sigma_{30}$
(−1,1,1)	Electric dipole 	$\rho(q_x,q_y)=\rho(-q_x,q_y)$	$\rho(q_x,q_y)\sim-\rho(q_x,-q_y)$	Σ_{23}
(1,−1,1)	Electric dipole 	$\rho(q_x,q_y)=\rho(q_x,-q_y)$	$\rho(q_x,q_y)\sim-\rho(-q_x,q_y)$	Σ_{21}
(−1,−1,1)	Electric quadruple 	$\rho(q_x,q_y)=\rho(-q_x,-q_y)$	$\rho(q_x,q_y)\sim-\rho(q_x,-q_y)$ $\rho(q_x,q_y)\sim-\rho(-q_x,q_y)$	Σ_{22}
(1,1,−1)	Magnetic quadruple 	$\rho(q_x,q_y)=\rho(-q_x,q_y)$ $\rho(q_x,q_y)=\rho(q_x,-q_y)$	$\rho(q_x,q_y)\sim 0$	Σ_{20}
(−1,1,−1)	Point spin 	$\rho(q_x,q_y)=\rho(-q_x,q_y)$ $\rho(q_x,q_y)=\rho(q_x,-q_y)$		$\Sigma_{03},\Sigma_{13},\Sigma_{33}$
(1,−1,−1)	Point spin 	$\rho(q_x,q_y)=\rho(-q_x,q_y)$ $\rho(q_x,q_y)=\rho(q_x,-q_y)$		$\Sigma_{01},\Sigma_{11},\Sigma_{31}$
(−1,−1,−1)	Point spin 	$\rho(q_x,q_y)=\rho(-q_x,-q_y)$		$\Sigma_{02},\Sigma_{12},\Sigma_{32}$

FIG. 1. (Color online) Different types of point impurities classified by whether they change sign under mirror symmetries and TRS. From the left: the η index, the possible physical realization, the exact symmetries of $\rho(\mathbf{q},\omega)$, the approximate symmetries of $\rho(\mathbf{q},\omega)$ to first order in V, and the corresponding $\Sigma_{\alpha\beta}$ in the four-band effective model (see text).

II. QUASIPARTICLE INTERFERENCE FOR TWO-DIMENSIONAL SYSTEMS WITH MIRROR SYMMETRIES AND TIME-REVERSAL SYMMETRY

We begin by considering a multiband homogeneous 2D system with the following symmetries: mirror reflections about xz and yz planes and TRS. In matrix representation, the single-particle Hamiltonian $H(\mathbf{k})$ and symmetry operators satisfy

$$\begin{aligned} M_{xz}H(k_x,k_y)M_{xz}^{-1} &= H(k_x,-k_y),\\ M_{yz}H(k_x,k_y)M_{yz}^{-1} &= H(-k_x,k_y),\\ U_T H(k_x,k_y)U_T^{-1} &= H^T(-k_x,-k_y), \end{aligned}$$

where $H(\mathbf{k})$ is written in an arbitrarily chosen orbital basis and M_{xz}, M_{yz}, and U_T ($T=KU_T$, with K being complex conjugation) are the unitary matrices representing the symmetry operations in the same basis. In the presence of impurities, the local density of states is defined as $\rho(\mathbf{r},\omega)=\sum_M |\langle\mathbf{r}|\psi_M\rangle|^2\delta(\omega-E_M)$, where $|\psi_M\rangle$ is the Mth single-particle eigenstate and E_M is the corresponding energy. Under Fourier transform, it becomes the FT-LDOS

$$\rho(\mathbf{q},\omega)=-\frac{1}{N\pi}\sum_{\mathbf{k}}\mathrm{Tr}[G(\mathbf{k},\mathbf{k}+\mathbf{q},\omega)-G^*(\mathbf{k}+\mathbf{q},\mathbf{k},\omega)], \tag{1}$$

where N is the total number of unit cells in the system, and $G(\mathbf{k},\mathbf{k}+\mathbf{q},\omega)$ is the retarded Green's function. For a single-point impurity given by a matrix V in the chosen basis, the exact T-matrix approach solves $G(\mathbf{k},\mathbf{k}+\mathbf{q},\omega)$ in terms of the homogeneous Green's function $G_0(\mathbf{k},\omega)$:

$$G(\mathbf{k},\mathbf{k}+\mathbf{q},\omega)=G_0(\mathbf{k},\omega)\delta_{\mathbf{q}0}+G_0(\mathbf{k},\omega)T(\omega)G_0(\mathbf{k}+\mathbf{q},\omega), \tag{2}$$

where $G_0(\mathbf{k},\omega)=(\omega-H(\mathbf{k})+i\eta)^{-1}$. The matrix $T(\omega)$ contains the effect of impurity and is defined as

$$T(\omega)=V\left(I-g(\omega)V\right)^{-1}, \tag{3}$$

where $g(\omega)=\sum_{\mathbf{k}}G_0(\mathbf{k},\omega)/N$. The pattern of $\rho(\mathbf{q},\omega)$ naturally depends on the type of impurity; namely, the form of matrix V. V is denoted by three indices (η_x,η_y,η_T), where $\eta_{x,y,T}=\pm1$ means that the impurity changes (does not change) sign under $M_{xz,yz}$ (TRS). For example, the combination $\eta=(1,-1,1)$ is an impurity that is invariant under mirror reflection about the xz plane and TRS yet changes sign under a mirror reflection about the yz plane. The physical realization of this type is an electric dipole oriented along the x axis. For any of the eight types, we derive the exact and approximate symmetries of $\rho(\mathbf{q},\omega)$ and summarize them in Fig. 1 (for derivation, see Appendix A). Here, "approximate"

indicates that the relation is valid only when $N_0(\omega)||V|| \ll 1$ where N_0 is the homogeneous density of states at ω.

Besides the global symmetries in $\rho(\mathbf{q},\omega)$ derived above, the most important feature of the FT-LDOS is the presence of *singularities* at certain scattering vectors; i.e., $\mathbf{q}$-vectors. We start from Eq. (2) by rewriting the retarded Green's function in terms of projectors:

$$\mathrm{Tr}[G(\mathbf{k},\mathbf{k}+\mathbf{q},\omega)] = \sum_{mn} \frac{\mathrm{Tr}[P_n(\mathbf{k}+\mathbf{q})P_m(\mathbf{k})T(\omega)]}{[\omega - E_m(\mathbf{k}) + i\eta][\omega - E_n(\mathbf{k}+\mathbf{q}) + i\eta]}, \quad (4)$$

where n is the band index and $P_n = |u_n(\mathbf{k})\rangle\langle u_n(\mathbf{k})|$ is the projector onto the nth band, and $|u_n(\mathbf{k})\rangle$ is the periodic part of the Bloch state at $\mathbf{k}$ with band index n. [In Eq. (4), we ignore the first term in Eq. (2) that gives the homogeneous DOS, as we are interested in the inhomogeneous part of the LDOS.] The most significant contribution to $\rho(\mathbf{q},\omega)$ comes from regions near the two poles of Eq. (2): at $\omega = E_m(\mathbf{k})$ and $\omega = E_n(\mathbf{k}+\mathbf{q})$, respectively. Physically, $\rho(\mathbf{q},\omega)$ comes from the elastic scattering between two states of energy ω possessing a momentum difference $\mathbf{k}_1 - \mathbf{k}_2 = \mathbf{q}$. From this picture, we know that the FT-LDOS is nonzero at $(\mathbf{q},\omega)$ if there are two states on the iso-energy contour of ω and separated by $\mathbf{q}$. In fact, closer study[10,24] shows that $\rho(\mathbf{q},\omega)$ is divergent at $\mathbf{q}$, if the normal directions, of the contour at $\mathbf{k}_1$ and $\mathbf{k}_2$, determined by the gradient of the dispersion, are parallel or antiparallel. As the gradient of dispersion is the quasiparticle group velocity, this shows that the forward (with zero scattering angle) and backward scattering (with π scattering angle) are the major channels. Any pair of $\mathbf{k}_1$ and $\mathbf{k}_2$ satisfying this condition are called a pair of stationary points denoted by $\mathbf{k}_{s1}$ and $\mathbf{k}_{s2}$, respectively, and generically $\rho(\mathbf{q},\omega)$ is divergent at $\rho(\mathbf{k}_{s1} - \mathbf{k}_{s2},\omega)$. Each divergence in reality becomes a finite peak due to finite quasiparticle lifetime [finite η in Eq. (4)]. The intensity of the peak is given by the prefactor $\mathrm{Tr}[P_n(\mathbf{k}_{s2})P_m(\mathbf{k}_{s1})T(\omega)]$ [see Eq. (4)]. When the two states at $\mathbf{k}_{s1}$ and $\mathbf{k}_{s2}$ are *orthogonal*, we have $\mathrm{Tr}[P_n(\mathbf{k}_{s2})P_m(\mathbf{k}_{s1})T(\omega)] = 0$ hence the peak at $\rho(\mathbf{k}_{s1} - \mathbf{k}_{s2},\omega) \sim 0$ is strongly suppressed. This *absence* of singularities in the FT-LDOS pattern is a symmetry-protected property of the system, because in general $\langle u_m(\mathbf{k}_{s1})|u_n(\mathbf{k}_{s2})\rangle = 0$ can only be guaranteed by the presence of an underlying symmetry. For example, in TRS topological insulator (TI), the two states at $\mathbf{k}$ and $-\mathbf{k}$ on the iso-energy contour are orthogonal because they are related by TRS. This leads to the suppression of $\rho(2\mathbf{k},\omega)$, which is a hallmark of TRS TI.[25,26] Mark that the suppression discussed here is completely independent of the symmetries of impurity, but only depends on the symmetries of the homogeneous system.

In a system with mirror symmetries M_{xz} and M_{yz}, M_{xz} (M_{yz}) ensures the orthogonality between two states with *different* eigenvalues of M_{xz} (M_{yz}), thus leading to forbidden scattering channels. In general, M_{xz} symmetry gives $E_n(k_x,k_y) = E_n(k_x,-k_y)$ and specially at $k_y = k_{inv}$ it gives $\partial_{k_y} E_n(k_x,k_{inv}) = 0$, where $k_{inv} = 0$ or π. Therefore, any two states on the iso-energy contour with $k_y = k_{inv}$ are a stationary pair. Additionally, as $[M_{xz}, H(k_x,k_{inv})] = 0$, these states are eigenstates of M_{xz}, having eigenvalue $\pm i$.[17] The general conclusion is that if the states at (k_1,k_{inv}) and (k_2,k_{inv}) have different mirror eigenvalues, the peak in the FT-LDOS at $(\pm(k_1 - k_2),k_{inv})$ is suppressed. The inverse statement is also true if the FT-LDOS due to stationary pair scattering at $(q,0)$ is suppressed, where $q = k_1 - k_2$ is the scattering vector between two states along $k_y = k_{inv}$, then states at (k_1,k_{inv}) and (k_2,k_{inv}) have opposite eigenvalues of M_{xz}. Similar statements can be made for the states along the k_y axis on the iso-energy contour at $k_x = k_{inv}$ by using M_{yz} symmetry.

Experimentally, the suppressed peaks in the FT-LDOS are observed by comparing them to the joint density of states (JDOS) $\rho_J(\mathbf{q},\omega)$ or the number of states per unit energy at energy ω and momenta $\mathbf{k}_1$ or $\mathbf{k}_2$ satisfying $\mathbf{k}_1 - \mathbf{k}_2 = \mathbf{q}$. The JDOS can be experimentally obtained by convolving the ARPES-measured spectral weight.[3] Formally, $\rho_J(\mathbf{q},\omega)$ is defined as

$$\rho_J(\mathbf{q},\omega) = -\frac{2}{N\pi}\mathrm{Im}\left[\sum_{m,n,\mathbf{k}} \frac{1}{[\omega - E_m(\mathbf{k}) + i\eta][\omega - E_n(\mathbf{k}+\mathbf{q}) + i\eta]}\right]. \quad (5)$$

When compared with Eq. (4), the only difference is that in $\rho_J(\mathbf{q},\omega)$ the factor $\mathrm{Tr}[P_m(\mathbf{k})T(\omega)P_n(\mathbf{k}+\mathbf{q})]$ is missing. Hence $\rho_J(\mathbf{q},\omega)$ is completely determined by the geometric features of the iso-energy contour. A comparison between $\rho(\mathbf{q},\omega)$ and $\rho_J(\mathbf{q},\omega)$ thus gives information on the wave functions, because any stationary vector that is present in $\rho_J(\mathbf{q},\omega)$ but absent in $\rho(\mathbf{q},\omega)$ indicates that the two wave functions at the contributing stationary points are orthogonal.

III. AN APPLICATION TO IDENTIFYING MIRROR-SYMMETRIC TOPOLOGICAL CRYSTALLINE INSULATOR

A. Absent peaks in FT-LDOS

We apply the general result to surface states of $Pb_{1-x}Sn_xTe$ to elucidate how its unique topological propertiesmanifest themselves in QPI. The surface states exist around $\bar{X}$ and $\bar{Y}$;[18–20] let us first focus on the states around $\bar{X}$ then, due to C_4 symmetry, a parallel analysis can be repeated for those around $\bar{Y}$. Along $\bar{\Gamma}\bar{X}\bar{\Gamma}$, there are two Dirac points (denoted by D_1 and D_2) or band crossings. Since the two band crossings have opposite eigenvalues of M_{xz}, and because TRS inverts M_{xz} eigenvalue from $\pm i$ to $\mp i$, the only possible configuration of M_{xz} eigenvalues is the one shown in Fig. 2(a), up to an overall sign. Besides the two Dirac points at the Fermi energy E_0, there are two additional Dirac points higher and lower than E_0 at $\bar{X}$ (denoted by D_3 and D_4). Along the perpendicular direction $\bar{M}\bar{X}\bar{M}$, however, there is no band-crossing point. Along this line, bands can either have the same eigenvalues of M_{yz} and hence repel each other [Fig. 2(b)], or they can have the same eigenvalue of M_{yz} but opposite effective mass [Fig. 2(c)]. D_3 and D_4 are protected by TRS and therefore

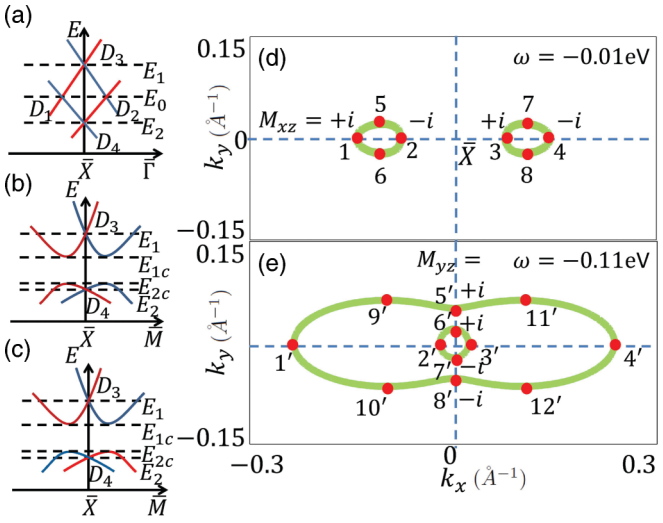

FIG. 2. (Color online) Schematic band dispersion of the surface bands at vicinity of $\bar{X}$ along (a) k_x axis and (b) k_y axis. Red and blue (lighter and darker gray, respectively) mean the band has eigenvalue $+i$ or $-i$, respectively, of M_{xz} in panel (a) and M_{yz} in panels (b) and (c). Iso-energy contour calculated for the model described in the text at $\omega = -0.01$ eV in panel (d) and $\omega = -0.11$ eV in panel (e). Eigenvalues of M_{xz} at points 1,2,3,4 are marked beside each point, and eigenvalues of M_{yz} at points 5′,6′,7′,8′ are similarly marked. The eigenvalues of M_{xz} at points 1′,2′,3′,4′ are identical to those at 1,2,3,4.

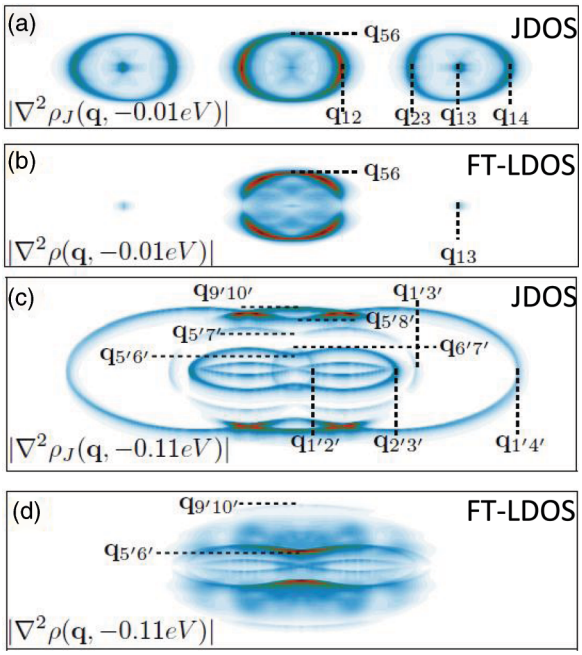

FIG. 3. (Color online) The absolute value of the divergence of the joint density of states, $|\nabla^2\rho_J(\mathbf{q},\omega)|$, is plotted for (a) $\omega = -0.01$ eV and (c) -0.11 eV. The absolute value of the divergence of the FT-LDOS around a static impurity potential $V = (0.1\text{ eV})\Sigma_{00}$, $|\nabla^2\rho(\mathbf{q},\omega)|$, is plotted for (b) $\omega = -0.01$ eV and (d) -0.11 eV.

appear in both directions; the other two Dirac nodes D_1 and D_2) are protected only by M_{xz} symmetry. To see the Lifshitz transition, we find that for $E_{2c} < \omega < E_{1c}$, the bands along $\bar{X}\bar{M}$ do not cross ω, resulting in an iso-energy contour of two separate ellipsoids centered at D_1 and D_2, respectively. From Fig. 2(a), along $\bar{X}\bar{\Gamma}$, the two points on the same side of $\bar{X}$ have opposite eigenvalues of M_{xz}. While for $\omega > E_{c1}$ or $\omega < E_{c2}$, the bands along $\bar{X}\bar{M}$ cross ω twice, resulting in an iso-energy contour of two concentric loops centered at $\bar{X}$. The two crossing points on same side of $\bar{X}$ have the same mirror eigenvalue according to Figs. 2(b) and 2(c). This analysis gives us the mirror eigenvalues on the iso-energy contours before and after the Lifshitz transition, marked in Figs. 2(d) and 2(e). We now use the general theory to obtain the following pairs of suppressed peaks in the FT-LDOS: $\mathbf{q}_{12}$, $\mathbf{q}_{34}$, and $\mathbf{q}_{23}$ before the Lifshitz transition ($\mathbf{q}_{ab}$ is defined as $\mathbf{q}_a - \mathbf{q}_b$), and $\mathbf{q}_{1'2'}$, $\mathbf{q}_{3'4'}$, $\mathbf{q}_{2'3'}$, $\mathbf{q}_{5'7'}$, $\mathbf{q}_{6'7'}$, and $\mathbf{q}_{5'8'}$ after the Lifshitz transition. We note that $\mathbf{q}_{14}$, $\mathbf{q}_{23}$, $\mathbf{q}_{1'4'}$, $\mathbf{q}_{2'3'}$, $\mathbf{q}_{5'8'}$, and $\mathbf{q}_{6'7'}$ are also forbidden by TRS because they are scattering vectors connecting Kramer's pairs in the presence of TRS.

B. Effective model and numerics

Thus far, we have extracted the symmetries of the single-impurity QPI pattern and located all vanishing singularities guaranteed by the presence of mirror symmetries, as one expects in $Pb_{1-x}Sn_xTe$. In order to be more concrete, we develop a minimal $\mathbf{k}\cdot\mathbf{p}$ model which qualitatively captures the surface-band dispersion both before and after the Lifshitz transition and calculate $\rho(\mathbf{q},\omega)$ around a point impurity (the most common impurity in $Pb_{1-x}Sn_xTe$). Near the Dirac points D_1 and D_2, the system can be approximated by two separate two-band $\mathbf{k}\cdot\mathbf{p}$ models. Nevertheless, in order to describe the Lifshitz transition where the two cones cross each other, one needs to consider the hybridization between the two cones and, thus, the minimal model is at least four band. At $\bar{X}$ there are two degenerate states at D_3 with $E_1 > E_0$ and two other degenerate states at D_4 with $E_2 < E_0$. Within each doublet, one is an eigenstate of M_{yz} with an eigenvalue of $+i$ while the other $-i$. We define our basis as $(1,0,0,0)$ and $(0,1,0,0)^T$; they have energy E_1 and mirror eigenvalues $M_{yz} = +i$ and $M_{yz} = -i$, respectively; $(0,0,1,0)^T$ and $(0,0,0,1)^T$ have energy E_2 and mirror eigenvalues of $M_{yz} = +i$ and $M_{yz} = -i$ respectively. There is gauge freedom in choosing the matrices for M_{xz} and U_T under this basis, and we choose $M_{xz} = i\Sigma_{01}$ and $U_T = i\Sigma_{02}$, where $\Sigma_{\alpha\beta} = \sigma_\alpha \otimes \sigma_\beta$. Applying symmetry constraints, we find that, to the linear order in $\mathbf{k}$, Σ_{30} and Σ_{10} couple to the zeroth order, $\Sigma_{01,11,31}$ couple to k_x and $\Sigma_{03,13,33}$ couple to k_y. The effective Hamiltonian can hence be written as

$$H(\mathbf{k}) = m\Sigma_{30} + m'\Sigma_{10} + (v_{1x}\Sigma_{01} + v_{2x}\Sigma_{11} + v_{3x}\Sigma_{31})k_x + (v_{1y}\Sigma_{03} + v_{2y}\Sigma_{13} + v_{3y}\Sigma_{33})k_y. \quad (6)$$

Qualitatively fitting the data for $Pb_{1-x}Sn_xTe$ given in Ref. 18, we choose the parameters in our Hamiltonian to be $\{m,m'\} = \{-0.11,-0.1\}$ eV, $\{v_{1x},v_{2x},v_{3y}\} = \{-1.5,-0.5,-3\}$ eV·Å and $\{v_{3x},v_{1y},v_{2y}\} \sim 0$. Here we define ~ 0 as being very small but nonzero in order to avoid accidental symmetries. We represent V for impurities with different η indices in a similar fashion using this basis, given in the last column of Fig. 1.

Using the effective Hamiltonian for $Pb_{1-x}Sn_xTe$, we calculate $\rho(\mathbf{q},\omega)$ with $V = (0.1\text{ eV})\Sigma_{00}$, i.e., a static point-charge impurity. In Figs. 3(b) and 3(d), we plot $|\nabla^2\rho(\mathbf{q},\omega)|$ at $\omega = -0.01$ eV and $\omega = -0.11$ eV, respectively. [$|\nabla^2\rho(\mathbf{q},\omega)|$

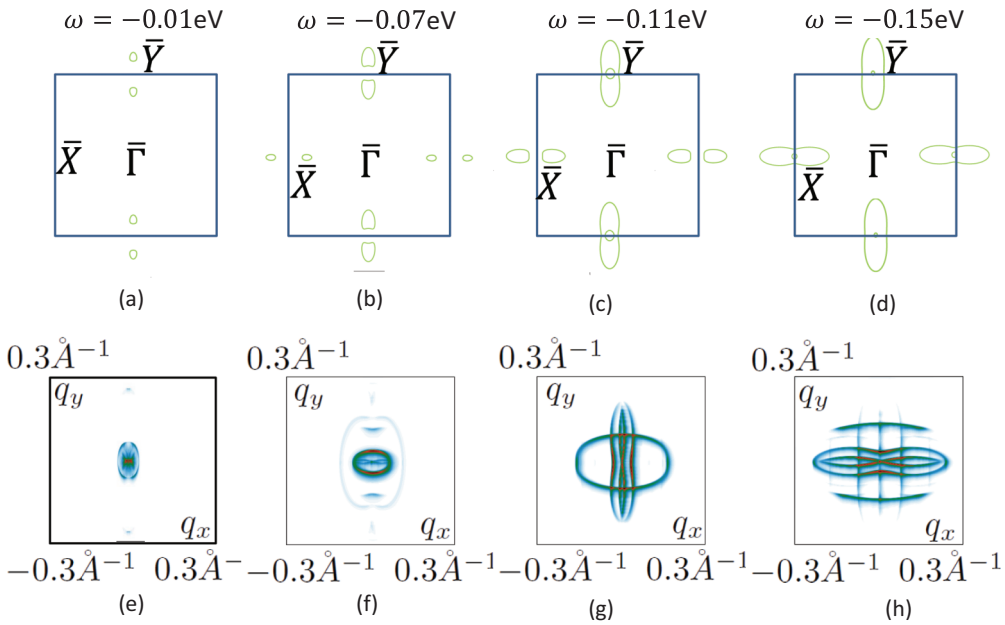

FIG. 4. (Color online) (a)–(d) The iso-energy contours at $\omega = -0.01$, -0.07, -0.11, and -0.15 eV, respectively, in the phase with rhombohedral distortion, breaking M_{xz} symmetry. (e)–(h) $\nabla^2\rho(\mathbf{q},\omega)$ calculated for the surface states in the rhombohedral phase around a single-charge impurity at the same energies listed above.

is plotted in lieu of $\rho(\mathbf{q},\omega)$ since it shows the singularities more clearly.] In comparison, we make the same plots for the JDOS, $|\nabla^2\rho_J(\mathbf{q},\omega)|$, in Figs. 3(a) and 3(c). In Figs. 3(a) and 3(c), we mark several $\mathbf{q}_s$ that join stationary $\mathbf{k}$ points marked in Fig. 2, and at all these vectors, there are peaks in $|\nabla^2\rho_J(\mathbf{q},\omega)|$. In contrast, in Figs. 3(b) and 3(d), we see that all peaks that are forbidden by either TRS or mirror symmetries vanish, confirming the previous analysis based on mirror eigenvalues of the $\mathbf{k}$ points.

C. Quasiparticle interference with rhombohedral distortion

In samples with $x \sim 1$ or pure SnTe, a spontaneous lattice distortion breaks one of the mirror symmetries (assumed to be M_{yz}) and C_4 symmetry. Assuming that the distortion breaks M_{xz}, we know that, first, the two Dirac nodes along $\bar{\Gamma}\bar{X}$ are no longer protected and open a gap of $2E_D$; second, the Lifshitz transition happens at two different energies, E_{cx} and E_{cy}, for the surface states around $\bar{X}$ and around $\bar{Y}$. As energy decreases from E_f, there are four phases: (i) no Fermi surface (FS) around $\bar{X}$ and two ellipsoids around $\bar{X}$ when $|\omega| < E_D$, (ii) two ellipsoids of FS around $\bar{X}$ and two other around $\bar{Y}$ when $E_D < |\omega| < |E_{cy}|$, (iii) two ellipsoids around $\bar{X}$ and two concentric loops around $\bar{Y}$ if $|E_{cy}| < |\omega| < |E_{cx}|$ and (iv) two concentric loops around $\bar{X}$ and two others around $\bar{Y}$ if $|\omega| > |E_{cx}|$. All these phases can be identified by QPI. In the pattern, all forbidden scattering vectors forbidden by M_{xz} are present while those forbidden by M_{yz} or TRS remain absent.

In the presence of the rhombohedral distortion, the fourfold rotation symmetry is broken and we have to consider the contribution from states near $\bar{X}$ and $\bar{Y}$ separately. Any term that breaks M_{xz} but preserves M_{yz} and TRS is of index $\eta = (-1,+1,+1)$. According to Fig. 1, in the effective theory around $\bar{X}$, this term is $\Delta\Sigma_{23}$. Without distortion, the effective theory around $\bar{Y}$ is obtained by rotating the model in Eq. (6) by $\pi/2$ and, in this theory, the distortion term corresponds to $\Delta\Sigma_{23}$. In Fig. 4, we choose $\Delta = 0.1$ eV and calculate the iso-energy contours at $\omega = -0.01$ eV in Fig. 4(a), -0.07 eV in Fig. 4(b), -0.11 eV in Fig. 4(c), and -0.15 eV in Fig. 4(d). From these figures, the change in the topology of the contours is clear: it changes from only two separate ellipsoids around $\bar{Y}$ in Fig. 4(a), to two separate ellipsoids around both $\bar{X}$ and $\bar{Y}$ in Fig. 4(b), to two separate ellipsoids around $\bar{X}$ and two concentric loops in Fig. 4(c), and finally to two concentric loops around both $\bar{X}$ and $\bar{Y}$ at highest ω in Fig. 4(d). The resultant QPI patterns $|\nabla^2\rho(\mathbf{q},\omega)|$ at these energies are plotted in Figs. 4(e)–4(h), respectively. These patterns are simply superpositions of patterns contributed by states around $\bar{X}$ and those around $\bar{Y}$; each pattern explicitly breaks fourfold rotational symmetry. Another important feature is that all $\mathbf{q}$ vectors that are forbidden by M_{xz} are now present. For example, in Fig. 4(f), the inner circle is contributed by the surface states around $\bar{X}$. On this circle, the left and right ends, defined as $\mathbf{q}_L$ and $\mathbf{q}_R$, are due to the scattering between $\mathbf{k}$s at the two ends of either one of the two pockets near $\bar{X}$. When M_{xz} is unbroken, these two $\mathbf{k}$s have opposite M_{xz} eigenvalues and hence scattering between them is forbidden. But with M_{xz} broken, $\mathbf{q}_L$ and $\mathbf{q}_R$ are allowed by symmetry. Compare this with Fig. 2(b); we can see that the distortion makes the intensity at $\mathbf{q}_L$ and $\mathbf{q}_R$ finite.

IV. DISCUSSION

The main results apply to any 2D or quasi-2D systems with mirror symmetries and, in a multi-orbital system, can be used to identify the orbital nature of the bands on an iso-energy contour. For example, by using our theory in conjunction with STS, one may use QPI to establish or disprove the

long-predicted Dirac metal state[27,28] in the spin-density wave (SDW) phase of the 1111 family of iron-based superconductors. When applying the theory to the cases where spin-orbital coupling is negligible (e.g., in iron-based superconductors) or, more accurately, where SU(2) symmetry is restored, we note the following differences: (i) mirror eigenvalues become real numbers ± 1 and (ii) there is no TRS forbidden channel due to spin degeneracy. Compared with ARPES with polarized light, which also resolves orbitals for bands lower than the Fermi energy in the absence of magnetic field, QPI can be applied to field-induced phases and to states above the Fermi energy.

In the application to $Pb_{1-x}Sn_xTe$, it is necessary to point out that we have assumed that $\rho(\mathbf{q},\omega)$ contains contributions only from scattering between states near $\bar{X}$. However, the full QPI pattern also consists of scattering among states near $\bar{Y}$ and interpocket scattering between states near $\bar{X}$ and those near $\bar{Y}$. Yet due to C_4 symmetry, the contribution to $\rho(\mathbf{q},\omega)$ made by states near $\bar{Y}$ can be obtained easily by making a fourfold rotation of $\rho(\mathbf{q},\omega)$ contributed by states around $\bar{X}$. The interscattering between states near $\bar{Y}$ and those near $\bar{X}$ only contributes to $\rho(\mathbf{q},\omega)$ near $\mathbf{q} \sim \bar{X} - \bar{Y} = (\pi,\pi)$. As these features are sufficiently separated in $\mathbf{q}$ space from those of in the small-$\mathbf{q}$ region, they are neglected in this work.

We have only studied the case of a single impurity, but the result extends to the case where there are random impurities of the same type and strength and when the impurity strength is weak. In Appendix B, we prove that, under these conditions, the FT-LDOS around a single impurity, $\rho(\mathbf{q},\omega)$, can be related to the autocorrelation function of the overall LDOS that results from many impurities, $R(\mathbf{r},\omega)$.

ACKNOWLEDGMENTS

C. F. is supported by ONR - N00014-11-1-0635 and N0014-11-1-0728. M. J. G. acknowledges support from the AFOSR under Grant No. FA9550-10-1-0459 and the ONR under Grant No. N0014-11-1-0728. B. A. B. was supported by NSF CAREER DMR- 095242, ONR - N00014-11-1-0635, Darpa - N66001-11- 1-4110, and the David and Lucile Packard Foundation.

APPENDIX A: DERIVATION OF GLOBAL SYMMETRIES OF $\rho(\mathbf{q},\omega)$ FOR DIFFERENT TYPES OF SINGLE IMPURITIES

In this section we explicitly derive the symmetries of $\rho(\mathbf{q},\omega)$, exact and approximate, listed in Fig. 1 of the main text for single impurities with eight possible η indices.

From Eq. (1), $\rho(\mathbf{q},\omega)$ is determined by the retarded Green's function $G(\mathbf{k},\mathbf{k}+\mathbf{q},\omega)$; yet from Eq. (2), $G(\mathbf{k},\mathbf{k}+\mathbf{q},\omega)$ is given in terms of the free-particle Green's function $G_0(\mathbf{k},\omega)$ and the T matrix, $T(\omega)$. The former has exactly the same symmetries as the homogenous Hamiltonian:

$$\begin{aligned} M_{xz}G_0(k_x,k_y,\omega)M_{xz}^{-1} &= G_0(k_x,-k_y,\omega),\\ M_{yz}G_0(k_x,k_y,\omega)M_{yz}^{-1} &= G_0(-k_x,k_y,\omega),\\ U_T G_0(\mathbf{k},\omega)U_T^{-1} &= G_0^T(-\mathbf{k},\omega). \end{aligned} \tag{A1}$$

The symmetries of $T(\omega)$, however, depends on symmetries of both the system *and* the impurity, i.e., the η index. Using definitions of η index and Eq. (3), one obtains

$$\begin{aligned} M_{xz}T(\omega)M_{xz}^{-1} &= \eta_x V[I-\eta_x g(\omega)V]^{-1} = T(\omega) \quad \text{if } \eta_x = 1 \sim -T(\omega) \quad \text{if } \eta_x = -1,\\ M_{yz}T(\omega)M_{yz}^{-1} &= \eta_y V[I-\eta_y g(\omega)V]^{-1} = T(\omega) \quad \text{if } \eta_y = 1 \sim -T(\omega) \quad \text{if } \eta_y = -1,\\ U_T T(\omega)U_T^{-1} &= \{\eta_T V[I-\eta_T g(\omega)V]^{-1}\}^T = T^T(\omega) \quad \text{if } \eta_T = 1 \sim -T^T(\omega) \quad \text{if } \eta_T = -1. \end{aligned} \tag{A2}$$

Here "$\sim$" means that the relation becomes exact only if $T(\omega)$ is replaced by its leading order, i.e., $T = V$.

Combining equations in Eqs. (A2), one easily obtains the other two equations:

$$(M_{xz}M_{yz})T(\omega)(M_{xz}M_{yz})^{-1} = \eta_x\eta_y V[I-\eta_x\eta_y g(\omega)V]^{-1} = T(\omega) \quad \text{if } \eta_x\eta_y = 1 \sim -T(\omega) \quad \text{if } \eta_x\eta_y = -1, \tag{A3}$$

$$\begin{aligned} (M_{xz}M_{yz}U_T)T(\omega)(M_{xz}M_{yz}U_T)^{-1} &= \{\eta_x\eta_y\eta_T V[I-\eta_x\eta_y\eta_T g(\omega)V]^{-1}\}^T\\ &= T^T(\omega) \quad \text{if } \eta_x\eta_y\eta_T = 1 \sim -T^T(\omega) \quad \text{if } \eta_x\eta_y\eta_T = -1. \end{aligned} \tag{A4}$$

Now we use Eqs. (A1) and (A2) and have

$$\begin{aligned} \rho(q_x,q_y,\omega) &= \frac{1}{N\pi}\sum_{\mathbf{k}}\left\{\mathrm{Tr}\left[M_{xz}G_0(k_x,k_y,\omega)T(\omega)G_0(k_x+q_x,k_y+q_y,\omega)M_{xz}^{-1}\right] - (\mathbf{q}\to-\mathbf{q})^*\right\}\\ &= \frac{1}{iN\pi}\sum_{\mathbf{k}}\left\{\mathrm{Tr}\left[G_0(k_x,k_y,\omega)M_{xz}T(\omega)M_{xz}^{-1}G_0(k_x+q_x,k_y-q_y,\omega)\right] - (\mathbf{q}\to-\mathbf{q})^*\right\}\\ &= \rho(q_x,-q_y,\omega) \quad \text{if } \eta_x = 1 \sim -\rho(q_x,-q_y,\omega) \quad \text{if } \eta_x = -1, \end{aligned} \tag{A5}$$

$$\begin{aligned} \rho(q_x,q_y,\omega) &= \frac{1}{iN\pi}\sum_{\mathbf{k}}\left\{\mathrm{Tr}\left[M_{yz}G_0(k_x,k_y,\omega)T(\omega)G_0(k_x+q_x,k_y+q_y,\omega)M_{yz}^{-1}\right] - (\mathbf{q}\to-\mathbf{q})^*\right\}\\ &= \frac{1}{iN\pi}\sum_{\mathbf{k}}\left\{\mathrm{Tr}\left[G_0(k_x,k_y,\omega)M_{yz}T(\omega)M_{yz}^{-1}G_0(k_x-q_x,k_y+q_y,\omega)\right] - (\mathbf{q}\to-\mathbf{q})^*\right\}\\ &= \rho(-q_x,q_y,\omega) \quad \text{if } \eta_y = 1 \sim -\rho(-q_x,q_y,\omega) \quad \text{if } \eta_y = -1, \end{aligned} \tag{A6}$$

$$\begin{aligned}\rho(q_x,q_y,\omega) &= \frac{1}{iN\pi}\sum_{\mathbf{k}}\left\{\mathrm{Tr}\left[U_T G_0(k_x,k_y,\omega)T(\omega)G_0(k_x+q_x,k_y+q_y,\omega)U_T^{-1}\right]-(\mathbf{q}\to-\mathbf{q})^*\right\}\\ &= \frac{1}{iN\pi}\sum_{\mathbf{k}}\left(\mathrm{Tr}\left\{G_0(-k_x-q_x,-k_y-q_y,\omega)\left[U_T T(\omega)U_T^{-1}\right]^T G_0(-k_x,-k_y,\omega)\right\}-(\mathbf{q}\to-\mathbf{q})^*\right)\\ &= \frac{1}{iN\pi}\sum_{\mathbf{k}}\left(\mathrm{Tr}\left\{G_0(k_x-q_x,k_y-q_y,\omega)\left[U_T T(\omega)U_T^{-1}\right]^T G_0(k_x,k_y,\omega)\right\}-(\mathbf{q}\to-\mathbf{q})^*\right)\\ &= \rho(q_x,q_y,\omega)\quad \text{if } \eta_T=1 \sim -\rho(q_x,q_y,\omega)\quad \text{if } \eta_T=-1. \end{aligned} \tag{A7}$$

We can also use Eqs. (A1) and Eqs. (A3) to obtain, very similarly,

$$\begin{aligned}\rho(q_x,q_y,\omega) &= \rho(-q_x,-q_y,\omega)\quad \text{if } \eta_x\eta_y=1\\ &\sim -\rho(-q_x,-q_y,\omega)\quad \text{if } \eta_x\eta_y=-1,\end{aligned} \tag{A8}$$

$$\begin{aligned}\rho(q_x,q_y,\omega) &= \rho(-q_x,-q_y,\omega)\quad \text{if } \eta_x\eta_y\eta_T=1\\ &\sim -\rho(-q_x,-q_y,\omega)\quad \text{if } \eta_x\eta_y\eta_T=-1.\end{aligned} \tag{A9}$$

Up to now we have derived all symmetries, exact and approximate, of $\rho(\mathbf{q},\omega)$ listed in Fig. 1.

APPENDIX B: AUTOCORRELATION OF $R(\mathbf{r},\omega)$ IN WEAK-IMPURITY LIMIT

In the text, we mention that, although we have only studied the case of a single impurity, the result extends to the case where there are random impurities of the same type and strength and when the impurity strength is weak. Here we prove that under these conditions, the FT-LDOS around a single impurity, $\rho(\mathbf{q},\omega)$, can be related to the autocorrelation function of the overall LDOS that results from many impurities, $R(\mathbf{r},\omega)$. By definition,

$$R(\mathbf{r},\omega)=\sum_n |\psi_n(\mathbf{r})|^2\delta(\omega-E_n)=-\frac{1}{\pi}\mathrm{Im}[G(\mathbf{r},\mathbf{r},\omega)], \tag{B1}$$

where $\psi_n(\mathbf{r})$ is an eigenfunction of the Hamiltonian, having eigenvalue E_n. The Fourier transform of $R(\mathbf{r})$ is, in terms of the retarded Green's function,

$$R(\mathbf{q},\omega)=\frac{1}{N\pi}\sum_{\mathbf{k}}\mathrm{Tr}[G(\mathbf{k},\mathbf{k}+\mathbf{q},\omega)-G^*(\mathbf{k}+\mathbf{q},\mathbf{k},\omega)], \tag{B2}$$

which is identical to the expression of $\rho(\mathbf{r})$ in the case of a single impurity. But now $G(\mathbf{k},\mathbf{k}+\mathbf{q},\omega)$ does not have a simple expression as in Eq. (3) in the text, since the system contains more than one impurity.

By definition, we have the Fourier transform of the correlation function $C(\mathbf{r})$ as (from here, we suppress the argument of ω for concision)

$$\begin{aligned}C(\mathbf{q}) &= \frac{1}{(2\pi)^3 N}\int d^3r' d^3r \langle R(\mathbf{r}+\mathbf{r}')R(\mathbf{r}')\exp(-i\mathbf{q}\cdot\mathbf{r})\rangle\\ &= \langle |R(\mathbf{q})|^2\rangle.\end{aligned} \tag{B3}$$

Therefore, the Fourier transform of the autocorrelation function $C(\mathbf{r})$ is exactly the ensemble average of the module squared Fourier component $R(\mathbf{q})$.

For an arbitrary configuration of identical impurities, the retarded Green's function is

$$\begin{aligned}G(\mathbf{k},\mathbf{k}+\mathbf{q}) &= G_0(\mathbf{k})\delta_{\mathbf{q}0}+G_0(\mathbf{k})V(\mathbf{q})G_0(\mathbf{k}+\mathbf{q})\\ &\quad+\frac{1}{N}\sum_{\mathbf{k}'}G_0(\mathbf{k})V(\mathbf{k}-\mathbf{k}')G_0(\mathbf{k}')V\\ &\quad\times(\mathbf{k}'-\mathbf{k}-\mathbf{q})G_0(\mathbf{k}+\mathbf{q})+\cdots,\end{aligned} \tag{B4}$$

where $V(\mathbf{q})=V\sum_i \exp(-i\mathbf{q}\cdot\mathbf{r}_i)$ is the Fourier transform of the impurity potential. From the above equation we have $R(\mathbf{q})$ as

$$\begin{aligned}R(\mathbf{q}) &= \rho_0\delta_{\mathbf{q}0}+\frac{1}{iN}\sum_{\mathbf{k}}\mathrm{Tr}[G_0(\mathbf{k})V(\mathbf{q})G_0(\mathbf{k}+\mathbf{q})-G_0^*(\mathbf{k}+\mathbf{q})V(\mathbf{q})G_0^*(\mathbf{k})]\\ &\quad+\frac{1}{iN^2}\sum_{\mathbf{k},\mathbf{k}'}\sum_{\mathbf{k}}\mathrm{Tr}[G_0(\mathbf{k})V(\mathbf{k}-\mathbf{k}')G_0(\mathbf{k}')V(\mathbf{k}'-\mathbf{k}-\mathbf{q})G_0(\mathbf{k}+\mathbf{q})\\ &\quad-G_0^*(\mathbf{k}+\mathbf{q})V(\mathbf{k}'-\mathbf{k}-\mathbf{q})G_0^*(\mathbf{k}')V(\mathbf{k}-\mathbf{k}')G_0^*(\mathbf{k})]+\cdots.\end{aligned} \tag{B5}$$

For $\mathbf{q}\neq 0$, the lowest order in $|\rho(\mathbf{q})|^2$ is the second order in V:

$$\begin{aligned}|R(\mathbf{q})|^2 &= \left|\mathrm{Tr}\left\{\frac{1}{N}\sum_{\mathbf{k}}[G_0(\mathbf{k})V(\mathbf{q})G_0(\mathbf{k}+\mathbf{q})-G_0^*(\mathbf{k}+\mathbf{q})V(\mathbf{q})G_0^*(\mathbf{k})]\right\}\right|^2\left|\sum_i\exp(-i\mathbf{q}\cdot\mathbf{r}_i)\right|^2\\ &= |\rho(\mathbf{q})|^2\left|\sum_i\exp(-i\mathbf{q}\cdot\mathbf{r}_i)\right|^2.\end{aligned} \tag{B6}$$

Finally, we use the independence (randomness) of the distribution of $\mathbf{r}_i$ to prove that

$$\left\langle \left| \sum_i \exp(-i\mathbf{q}\cdot\mathbf{r}_i) \right|^2 \right\rangle = N_i + \sum_{i\neq j} \langle \exp[i\mathbf{q}\cdot(\mathbf{r}_j - \mathbf{r}_i)] \rangle = N_i,$$

where N_i is the total number of impurities. Up to this point, we have proved that the Fourier transform of the autocorrelation function $C(\mathbf{r})$ of the overall LDOS $R(\mathbf{r})$ is proportional to $|\rho(\mathbf{q})|^2$ in the limit of weak impurities. In other words, the singularities in $\rho(\mathbf{q})$ can be revealed in the autocorrelation of LDOS in the case of multiple identical impurities.

[1] K. McElroy, R. W. Simmonds, J. E. Hoffman, D.-H. Lee, J. Orenstein, H. Eisaki, S. Uchida, and J. C. Davis, Nature (London) **422**, 592 (2003).

[2] P. Aynajian, E. H. da Silva Neto, A. Gyenis, R. E. Baumbach, J. D. Thompson, Z. Fisk, E. D. Bauer, and A. Yazdani, Nature (London) **486**, 201 (2012).

[3] P. Roushan, J. Seo, C. V. Parker, Y. S. Hor, D. Hsieh, D. Qian, A. Richardella, M. Z. Hasan, R. J. Cava, and A. Yazdani, Nature (London) **460**, 1106 (2009).

[4] T. Zhang, P. Cheng, X. Chen, J.-F. Jia, X. Ma, K. He, L. Wang, H. Zhang, X. Dai, Z. Fang, X. Xie, and Q.-K. Xue, Phys. Rev. Lett. **103**, 266803 (2009).

[5] J. Seo, P. Roushan, H. Beidenkopf, Y. S. Hor, R. J. Cava, and A. Yazdani, Nature (London) **466**, 343 (2010).

[6] Y. Okada, C. Dhital, W. Zhou, E. D. Huemiller, H. Lin, S. Basak, A. Bansil, Y.-B. Huang, H. Ding, Z. Wang, S. D. Wilson, and V. Madhavan, Phys. Rev. Lett. **106**, 206805 (2011).

[7] Z. Alpichshev, J. G. Analytis, J.-H. Chu, I. R. Fisher, Y. L. Chen, Z. X. Shen, A. Fang, and A. Kapitulnik, Phys. Rev. Lett. **104**, 016401 (2010).

[8] Z. Alpichshev, J. G. Analytis, J.-H. Chu, I. R. Fisher, and A. Kapitulnik, Phys. Rev. B **84**, 041104 (2011).

[9] C. Bena, Phys. Rev. B **79**, 125427 (2009).

[10] Q. Liu, X.-L. Qi, and S.-C. Zhang, Phys. Rev. B **85**, 125314 (2012).

[11] A. P. Schnyder, S. Ryu, A. Furusaki, and A. W. W. Ludwig, Phys. Rev. B **78**, 195125 (2008).

[12] L. Fu, Phys. Rev. Lett. **106**, 106802 (2011).

[13] T. L. Hughes, E. Prodan, and B. A. Bernevig, Phys. Rev. B **83**, 245132 (2011).

[14] A. M. Turner, Y. Zhang, R. S. K. Mong, and A. Vishwanath, Phys. Rev. B **85**, 165120 (2012).

[15] T. Hsieh, H. Lin, J. Liu, W. Duan, A. Bansil, and L. Fu, Nat. Commun. **3**, 982 (2012).

[16] C. Fang, M. J. Gilbert, X. Dai, and B. A. Bernevig, Phys. Rev. Lett. **108**, 266802 (2012).

[17] C. Fang, M. J. Gilbert, and B. A. Bernevig, Phys. Rev. B **86**, 115112 (2012).

[18] S.-Y. Xu, C. Liu, N. Alidoust, D. Qian, M. Neupane, J. D. Denlinger, Y. J. Wang, L. A. Wray, R. J. Cava, H. Lin, A. Marcinkova, E. Morosan, A. Bansil, and M. Z. Hasan, Nat. Commun. **3**, 1192 (2012).

[19] P. Dziawa, B. J. Kowalski, K. Dybko, R. Buczko, A. Szczerbakow, M. Szot, E. Ausakowska, T. Balasubramanian, B. M. Wojek, M. H. Berntsen, O. Tjernberg, and T. Story, Nat. Mater. **11**, 1023 (2012).

[20] T. Tanaka, Z. Ran, T. Sato, K. Nakayama, S. Souma, T. Takahashi, K. Segawa, and Y. Ando, Nat. Phys. **8**, 800 (2012).

[21] M. Kargarian and G. A. Fiete, Phys. Rev. Lett. **110**, 156403 (2013).

[22] J. Liu, W. Duan, and L. Fu, arXiv:1304.0430 (2013).

[23] C.-X. Liu, arXiv:1304.6455 (2013).

[24] R. R. Biswas and A. V. Balatsky, Phys. Rev. B **81**, 233405 (2010).

[25] X. Zhou, C. Fang, W.-F. Tsai, and J. P. Hu, Phys. Rev. B **80**, 245317 (2009).

[26] W.-C. Lee, C. Wu, D. P. Arovas, and S.-C. Zhang, Phys. Rev. B **80**, 245439 (2009).

[27] Y. Ran, F. Wang, H. Zhai, A. Vishwanath, and D.-H. Lee, Phys. Rev. B **79**, 014505 (2009).

[28] M. Z. Hasan and B. A. Bernevig, Physics **3**, 27 (2010).